Molybdenum disulfide nanoflowers mediated anti-inflammation macrophage modulation for spinal cord injury treatment

Guodong Sun[1,#], Shuxian Yang[1,#], Huaihong Cai[2,#], Yijin Shu[2], Qi Han[3], Baocheng Wang[1], Zhizhong Li[4], Libing Zhou[5], Qingsheng Gao[2,*], Zhinan Yin[1,*]

1. The First Affiliated Hospital, Biomedical Translational Research Institute, Jinan University, Guangzhou 510632, P. R. China.
2. College of Chemistry and Materials Science, Jinan University, Guangzhou 510632, P. R. China.
3. Spinal Cord and Brain Injury Research Group, Stark Neurosciences Research Institute, Department of Neurological Surgery, Goodman Campbell Brain and Spine, Indiana University School of Medicine, Indianapolis, IN 46202, United States.
4. The First Affiliated Hospital, Jinan University, Guangzhou 510632, P. R. China.
5. Guangdong-Hongkong-Macau Institute of CNS Regeneration, Ministry of Education CNS Regeneration Collaborative Joint Laboratory, Jinan University, Guangzhou 510632, P. R. China.

# These authors contributed equally to this work.

* Corresponding authors: Dr. Qingsheng Gao (tqsgao@jnu.edu.cn) and Dr. Zhinan Yin (zhinan.yin@yale.edu)

Abstract:

Spinal cord injury (SCI) can cause locomotor dysfunctions and sensory deficits. Evidence shows that functional nanodrugs can regulate macrophage polarization and promote anti-inflammatory cytokine expression, which is feasible in SCI immunotherapeutic treatments. Molybdenum disulfide (MoS_2) nanomaterials have garnered great attention as potential carriers for therapeutic payload. Herein, we synthesize MoS_2@PEG (MoS_2 = molybdenum disulfide, PEG = poly (ethylene glycol)) nanoflowers as an effective carrier for loading etanercept (ET) to treat SCI.

We characterize drug loading and release properties of MoS_2@PEG *in vitro* and demonstrate that ET-loading MoS_2@PEG obviously inhibits the expression of M1-related pro-inflammatory markers (TNF-α, CD86 and iNOS), while promoting M2-related anti-inflammatory markers (Agr1, CD206 and IL-10) levels. *In vivo*, the mouse model of SCI shows that long-circulating ET-MoS_2@PEG nanodrugs can effectively extravasate into the injured spinal cord up to 96 hours after SCI, and promote macrophages towards M2 type polarization. As a result, the ET-loading MoS_2@PEG administration in mice can protect survival motor neurons, thus, reducing injured areas at central lesion sites, and significantly improving locomotor recovery. This study demonstrates the anti-inflammatory and neuroprotective activities of ET-MoS_2@PEG and promising utility of MoS_2 nanomaterial-mediated drug delivery.

1. Introduction

Traumatic spinal cord injury (SCI) is a major medical problem worldwide, often resulting in motor dysfunction and chronic pain syndrome. Among the physiopathological mechanisms involved in the progression of SCI, inflammation is one of the most relevant factors. Extensive research has shown that acute inflammation, characterized by immune cell activation and inflammatory cytokine release, can result in extensive tissue damage, eventually leading to chronic and persistent pain syndrome [1]. Accumulating evidence shows that macrophages play key cellular roles in inflammatory events [2]. Therefore, regulating inflammation through modulating activated macrophages is a promising strategy for SCI treatment [3].

Macrophage activation is associated with distinct macrophage phenotypes, *i.e.*, pro-inflammatory (M1) and anti-inflammatory (M2) macrophages. Pro-inflammatory M1 macrophages can secrete inflammatory cytokines, such as tumor necrosis factor-α (TNF-α), interferon-γ (INF-γ), and interleukins (IL) -2, -6, and -8 [4-6]. However, anti-inflammatory M2 macrophages can regulate immune inflammatory reactions,

promote tissue reconstruction, and repair autonomic functions [7]. Therefore, blocking M1 macrophage activation pathways and further reprogramming macrophages toward M2 phenotypes will be feasible in new immunotherapeutic treatments for SCI [5,7]. The current clinical treatment using high-dose anti-inflammatory drugs is controversial because of deleterious side effects [8]. Thus, it is still a challenge to develop a new anti-inflammatory drug candidate that effectively modulates inflammation at SCI sites and minimizes side effects.

Nanomaterial-based drug carriers are promising candidates for modulating inflammation *in situ* at SCI sites [9-12]. Recent evidence *in vitro* and *in vivo* suggests that nanoparticles can disrupt vasculatures at SCI sites, and then effectively enhance site-specific drug delivery efficacy [13-15]. Two-dimensional (2D) transition metal dichalcogenides (TMDs) nanomaterials, e.g., molybdenum disulfide (MoS_2), have emerged as important segments to construct nanocarriers in drug delivery, because of their good biocompatibility and intercalatable structures [16-18]. However, there is no relevant report about fabricating MoS_2-based nanocarriers for SCI treatments. Considering the rich unsaturated-sites of Mo and S on MoS_2 surfaces and their subsequently strong interactions with cells, MoS_2 mediated anti-inflammatory macrophage modulations may be effective in SCI treatments, which is presently unknown. In this work, the clinical treatment anti-inflammatory drug etanercept (ET), considered relatively safe, was chosen to fabricate a new type of nanodrug through combining with MoS_2 nanosheets. ET is an inhibitor for TNF-α, a key anti-inflammatory cytokine immunity regulator [19]. Thus, blocking the activity of pro-inflammatory cytokines might be beneficial in SCI treatment because it could confer neuroprotection and aid in locomotor recovery [20]. This represents an attractive strategy to exploit well-designed MoS_2 nanocarrier loading anti-inflammatory drugs, such as Trojan Horse for lengthening therapeutic time-windows and minimizing high-dose drug administration in SCI treatments.

In this study, we designed MoS_2@PEG nanoflowers evenly integrating poly (ethylene glycol) (PEG) with MoS_2 nanosheets as feasible nanocarriers for loading the anti-inflammatory drug ET (Scheme 1a). The ET-loading MoS_2@PEG remarkably

promotes locomotor recovery in mice at post-SCI by inducing an anti-inflammatory immune response with M2 macrophage polarization *in vivo* and *in vitro* (Scheme 1b). More importantly, the time-window for injection at post-injuryis expanded to more than 96 hours after ET-loading MoS_2@PEG administration, which is of great importance in clinical post-SCI treatments. This work presents a novel MoS_2 nanocarrier-mediated drug delivery strategy to selectively modulate anti-inflammatory events and promote locomotor recovery in SCI treatments.

2. Experimental section

2.1. Materials and reagents

Ammonium heptamolybdatetetrahydrate $((NH_4)_6Mo_7O_{24}\cdot4H_2O)$, thiourea $(CS(NH_2)_2)$, and poly(ethylene glycol)-600 (PEG) were purchased from Sinopharm Chemical Reagent Co., Ltd. (Shanghai, China). The recombinant human tumor necrosis factor-α receptor IgG Fc fusion protein (rhTNFR:Fc), which was also called etanercept (ET), was obtained from Shanghai CP Guojian Pharmaceutical Co., Ltd (Shanghai, China). All the other chemicals were of analytical grade and used as received without further purification. Primary antibodies, including rabbit anti mouse GFAP (ab7260), rat anti mouse F4/80 (ab90247), rabbit anti-Nitric oxide synthase (iNOS; ab15323), and mouse anti-Arg1 (ab212522), were all purchased from Abcam (Cambridge, MA, USA). Lipopolysaccharides (LPS) from Escherichia coli O111:B4 was purchased from Sigma-Aldrich (Shanghai, China). All aqueous solutions were prepared using ultrapure water (> 18 MΩ).

2.2 Characterization

The morphology of nanomaterials was characterized by transmission electron microscope (TEM) (JEM-2100F, JEOL). X-ray diffraction (XRD) was performed on a Bruker D8 diffractometer, using Cu-Kα radiation (λ = 1.54056 Å). Fourier transform infrared spectroscopy (FT-IR) was performed with a Nicolet 6700 FT-IR spectrometer. The cell imaging was observed by laser scanning confocal microscope (LCM-510, Carl Zeiss).

2.3 Synthesis of ET-loading MoS$_2$@PEG nanoflowers

The MoS$_2$@PEG nanoflowers were synthesized via a microwave-assisted hydrothermal route according to our previous report [21]. Typically, 0.353 g of (NH$_4$)$_6$Mo$_7$O$_{24}$·4H$_2$O, 1.83 g of TU, and 0.06 g of PEG-600 were dissolved in 15 mL of distilled water; then the solution was placed in a microwave reactor (Preekem MX-8000, Shanghai). After microwave irradiation at 220 $^{\circ}$C for 10 minutes, the as-prepared MoS$_2$@PEG was collected by centrifugation, thoroughly washed with distilled water for three times, and dried at 50 $^{\circ}$C. For drug loading, 50 μg ET was first added to 1 mL MoS$_2$@PEG (0.1 mg/mL) and reacted overnight. After reaction, the mixture was dialyzed with distilled water for 24 hours using dialysis membrane (MW cutoff = 3000); then the synthesized ET-loading MoS$_2$@PEG was re-dispersed in 1 mL phosphate-buffered saline (PBS) (pH 7.4), then stored at 4 $^{\circ}$C for further use.

2.4. *In vitro* study

2.4.1. Cell culture and MTT assay

The RAW 264.7 macrophages from mouse and the bone marrow stem cells (BMSC) from human were obtained from the Life Science Research Institute of the Cell Resource Centre (Shanghai, China). The cells were cultured in the DMEM medium supplemented with 10% fetal bovine serum (FBS) and 1% penicillin/streptomycin in 5% CO$_2$-humidified chamber at 37°C in CO$_2$ incubator (95% relative humidity, 5% CO$_2$).

Cell viability was evaluated by MTT assay. Different types of cells, including RAW 264.7 and BMSC, were cultivated in 96-well plates for 24 hours. Subsequently, the medium was substituted for fresh medium, supplemented with different concentrations of MoS$_2$ nanosheets, MoS$_2$@PEG nanoflowers, and ET-MoS$_2$@PEG, respectively. After 24 hours of incubation, cells were washed with PBS (pH 7.4) twice and incubated with 0.5 mg/mL 3-(4,5-dimethyl-2-thiazolyl)-2,5-diphenyl -2-H-tetrazolium bromide (MTT) reagent at 37 $^{\circ}$C for 4 h. The absorbance was measured at 490 nm using an absorbance microplate reader.

2.4.2 Cellular Uptake of MoS$_2$@PEG

Cellular uptakes of nanoparticles were examined by labeling MoS$_2$@PEG by green fluorescence protein (GFP). For fabricating GFP-labeled MoS$_2$@PEG, 100 μL of GFP (1 mg/mL, DMSO) was added drop by drop to 1 mL of MoS$_2$@PEG solution, then reacted in the dark for 6 hours. After reaction, the mixture was dialyzed with distilled water for 24 hours using dialysis membrane (MW cutoff = 3000), following which GFP-labeled MoS$_2$@PEG was obtained.

For cell cultures, macrophages were seeded in a 6-well culture plate at a density of 1×10^5 cells/well and allowed to adhere for 24 hours. Then, the old medium was replaced by the medium with GFP-labeled MoS$_2$@PEG. After incubation for 2 h at 37 °C, cells were washed for three times with cell medium, then fixed with 4% paraformaldehyde for 20 minutes. For cell staining, cells were incubated with 1 μg/mL of anti-F4/80 antibody (specific targeting to macrophages) for 1 h and 1 μg/mL of DAPI (specific targeting to cell nucleus) for 30 minutes at 37 °C. The stained cells were washed with PBS (pH 7.4) for three times and observed by fluorescence microscope with 488 nm excitation.

2.4.3. *In vitro* ET loading and release of MoS$_2$@PEG

For investigating drug-loading capacity of MoS$_2$@PEG, 1 mL MoS$_2$@PEG (0.1 mg/mL) was incubated with 50 μg ET overnight. Following incubation, the ET-loading MoS$_2$@PEG was centrifuged at 5000 rpm for 10 minutes. The amount of ET loaded was calculated by abcam's Etanercept ELISA Kit (ab237643) following the manufacturer's protocol.

For drug release study, 10 mL of ET-MoS$_2$@PEG solution was placed into dialysis membrane (MW cutoff = 3000) and dialyzed against 250 mL of distilled water at room temperature. Aliquots of 2.0 mL were withdrawn from the solution at different intervals (0, 4, 8, 12, 24, 48, 72, 96, 120 and 144 hours). The volume of solution was maintained constantly by adding 2.0 mL of PBS (pH 7.4) after each sampling. The amount of ET released from MoS$_2$@PEG was measured using abcam's Etanercept ELISA Kit (ab237643) following the manufacturer's protocol. These experiments were repeated for three times and the drug releasing kinetics were plotted based on obtained results. In the control group, ET release from MoS$_2$ nanosheets was

examined by fabricating of ET-loading MoS_2 nanosheets firstly. For preparing ET-loading MoS_2 nanosheets, 50 μg ET was first added to 1 mL MoS_2 nanosheets (0.1 mg/mL) and this mixed solution was reacted overnight. After reaction, the mixture was dialyzed with distilled water for 24 hours using dialysis membrane (MW cutoff = 3000), and then ET-loading MoS_2 nanosheets were obtained. The experiment procedure of ET release from MoS_2 nanosheets was in accordance with the above.

2.4.3. Macrophage activation

Macrophages were activated with lipopolysaccharides (LPS), which is a well-known agent for stimulating macrophage activation *in vitro* and *in vivo* [22]. Briefly, macrophages were cultured at a density of 10^6 cells/well overnight. Macrophages were activated by 100 ng/ml of LPS for 18 hours, and cells were washed for three times with cell medium. Subsequently, cells were incubated with different agents (ET, MoS_2@PEG, and ET-MoS_2@PEG) containing media for 6 hours; then cells were washed for three times with PBS (pH 7.4) and collected for cytokine assays.

2.5. *In vivo* study

2.5.1 Contusive SCI model

Animal experiments were performed according to the Guidelines for the Care and Use of Laboratory Animals, which was approved by the Animal Care and Use Committee of Jinan University (Guangzhou, China). Adult female C57BL/6J mice (7-8 weeks old, weights of 17-22g) were purchased from Guangdong Medical Laboratory Animal Center Co., Ltd., and housed in room temperature and humidity controlled animal quarters under a 12 hour light/dark cycle.

The mice were deeply anesthetized by isoflurane vapor (3%). The contusive SCI model was constructed using the New York University Impactor equipped for mouse contusion surgeries. Spinal cords were exposed by laminectomy at T11-12 levels and contused by a 10 g rod dropped at a distance of 6.25 mm.

2.5.2 Administration of MoS_2@PEG and ET-MoS_2@PEG

After 48 hours post SCI, nanomaterials were delivered intravenously in mice via the tail vein. The mice (n = 6 ~ 8 animals per experimental group) were transcardially

perfused after post-injections. The spinal cord sections were then saved for genomic analysis, histochemical, and immunofluorescent staining.

2.5.3 Spinal cord tissue processing

Mice spinal cord tissues were resected after post SCI at 8 weeks. The mice were deeply anesthetized with pentobarbital (50 mg/kg), following thoracotomy. Then 30 mL of normal saline was rapidly perfused through their left ventricles, and 30 mL 4% paraformaldehyde was used for fixation. Spinal cord segments of 5 mm in length were resected from T11 transition level vertebral of mice and soaked in 4% paraformaldehyde for 24 hours. The spinal cord segments were transferred into 30% sucrose solution before the tissues sank. Finally, the tissues were cut into 20 μm sections after freezing.

2.5.4 Assessment of locomotor capacity and motor evoked potential (MEP) detection

Locomotion recovery after SCI was scored according to the Basso Mouse Scale (BMS) [23] and CatWalk-assisted gait analysis [24]. Two independent examiners blinded to the treatment regimen assessed hind limb movements.

Motor evoked potential (MEP) testing was carried out by electromyography on post-SCI mice. A stimulation electrode was applied to the rostral ends of their surgical spinal cords and the recording electrode was placed in their biceps flexor cruris. A single square wave stimulus was 0.5 mA, 0.5 ms in duration, 2 ms time delay, and 1 Hz. The amplitude was measured from the initiation point of the first response wave to its highest point.

2.5.5 Acute toxicity experiments

After administration of MoS_2@PEG and ET-MoS_2@PEG, the treated-mice in different groups were sacrificed after 21 days. The organs, including heart, liver, spleen, lungs, and kidneys, were acquired, fixed with formalin, embedded with paraffin, and sectioned. 0.8 mL of blood samples was collected from each mouse to conduct blood analysis and serum biochemistry assay.

2.5.6 Nanoparticle extravasation study

At different time points (24, 48, and 96 hours and 1 week), the mice were intravenously administered a 200 μL GFP-labeled MoS$_2$@PEG. They were then sacrificed after nanomaterial injection. Spinal cords were dissected out and postfixed overnight in 4% PFA in PBS and, subsequently, in 30% sucrose solution in PBS for 48 hours for cryoprotection, after which spinal cords were frozen and prepared for cryosection.

2.5.7 Histology and immunohistochemistry

The 20 μm-thick serial frozen sections of spinal cords were stained with 0.1% cresyl violet to image tissue morphology. The 5 μm-thick paraffin sections of organ tissues were stained with Hematoxylin and Eosin (H&E) staining solution. For imunohistochemistry, the RAW 264.7 cells were fixed with 4% paraformaldehyde and permeabilized by 0.2% Triton X-100 (Sigma-Aldrich). Staining was carried out by overnight with the primary antibodies, including anti-F4/80 (1:1000, ab90247), anti-CD11b (1:200, ab8878), anti-CD11c (1:200, ab11029), anti-CD206 (1:200, ab64693), anti-iNOS (1:100, ab15323), anti-Arg1 (1:100, ab212522), and anti-GFAP(1:1000, ab7260). For fluorescent imaging, fluorescent Alexa Fluor 488 or 546 secondary antibodies (1:1000, Invitrogen) were used for staining at room temperature for 2 h. After PBS washing, the tissue slices were fixed with Vectashield containing DAPI and used for fluorescent imaging. Inverted fluorescence microscope (Axio Observer A1, carl zeiss, Germany) was used for imaging and fluorescence analysis.

2.5.8 Spinal cord tissue immunofluorescence

Briefly, the mice were anesthetized using pentobarbital (50 mg/kg) and perfused with 0.1 M PBS, followed by 4% PFA. After a laminectomy, a 10 mm segment at T11 vertebrae was cut and the tissue samples were quickly frozen in an ethanol-dry ice bath. Samples were then stored at -80°C, and homogenized in a 200 μL ice-cold Cell Lysis Buffer (Beyotime, China) containing enzyme inhibitors. Subsequently, the samples were centrifuged at 10,000 g for 10 minutes at 4 °C, after which, the supernatants were frozen at -80 °C. Protein levels were then determined using bicinchoninic acid (BCA) protein assay (Beyotime, China).

The spinal cords from mice were analyzed with the Bio-Plex system (Bio-Rad, Hercules, CA) using a 23-plex cytokine array kit, including Eotaxin, G-CSF, GM-CSF, IFN-γ, IL-1α, IL-1β, IL-2, IL-3, IL-4, IL-5, IL-6, IL-9, IL-10, IL-12, IL-12, IL-13, IL-17A, KC, MCP-1 (MCAF), MIP-1α, MIP-1β, RANTES, and TNF-α.

2.5.9 Pathology analysis

Mice were sacrificed, and tumors were set in 4% paraformaldehyde solution for fixing, set in paraffin, and stained with hematoxylin and eosin (H&E). The slice was examined with an inverted luminescence microscope (OLYMPUS X73, Japan).

2.6 Statistical analysis

Data were expressed as mean ± standard deviation for at least three independent experiments. The Student's *t* test was used to assess the significance between experimental and control groups. Values were considered significant at $p < 0.05$.

3.   Results and discussion

3.1. ET-loading MoS$_2$@PEG nanoflowers synthesis and characterization

In this study, the MoS$_2$@PEG nanocomposites were synthesized via a microwave-assisted hydrothermal process (Scheme 1a). Regarding the abundant PEG in the MoS$_2$@PEG and its rich ether and hydroxyl groups, ET could be combined on nanoflower surfaces through noncovalent approach (*e.g.*, hydrogen bonds, van der Waals force, *etc*.). Such weak interactions were beneficial for the release of ET during treatments. As observed in TEM image (Figure 1a), the synthesized MoS$_2$@PEG presented a size of 200 - 300 nm. Closer observation showed that the nanocomposite had a flower-like structure, and its visible lattice fringes were measured at 0.27 nm (Figure 1b), which could be indexed as the (100) or (010) of hexagonal MoS$_2$. This result was in good accordance with XRD analysis (Figure 1c). Collectively, TEM image validated that MoS$_2$@PEG nanoflowers consisted of multi-layers of MoS$_2$ nanosheets. The FT-IR spectrum showed the absorption bands associated with v_{O-H} (3413 cm^{-1}), $v_{C=S}$ (1400 cm^{-1}) and δ_{N-H} (619 cm^{-1}) (Figure 1d), identifying the presence of PEG in the composites. Noticeably, the obvious v_{O-H} band indicated the rich hydroxyl groups on MoS$_2$@PEG surfaces, which were absent on bare MoS$_2$ nanosheets.

We next investigated the ET-loading capacity of MoS_2@PEG nanoflowers and bare MoS_2 nanosheeets. As shown in Figure 1e, ET loading on MoS_2@PEG was significantly higher (~60% of total ET added) compared with the MoS_2 nanosheets (~30% of total ET addition). This suggested that the flower-like nanostructure had a higher drug loading capacity, which was an additional advantage of our technique. Furthermore, their releasing kinetics was shown in Figure 1f. Visibly, the MoS_2@PEG displayed a slower rate of ET release; only ~45% of the drug was released after 24 hours, and almost 100% was after 144 hours. By contrast, the MoS_2 nanosheets released ~60% ET in the first 12 hours and ~80% after 24 hours, while almost 100% after 75 hours (Figure 1f). As for the MoS_2@PEG, the relatively rapid release observed in the initial period could be attributed to the diffusion of ET loaded on nanosheet surfaces. Subsequently, the slower release after 24 hours was ascribed to this building-block structure, in which drugs were entrapped between layers of MoS_2 nanosheets. Therefore, this nanoflower structure of MoS_2@PEG and weak noncovalent interactions with ET provided a facile strategy to tune the drugs' releasing capabilities.

3.2. *In vitro* cell viability and *in vivo* toxicity evaluation

To meet the requirements of biomedical application, it was essential to examine the toxicity of the nanocarriers. The cell viabilities of MoS_2 nanosheets, MoS_2@PEG, ET, and ET-MoS_2@PEG at different concentrations were evaluated using different cell lines (including RAW 264.7 and BMSC), respectively. As shown in Figure 2, the low level of cytotoxixity (~90% cell viability) was observed for MoS_2 nanosheets, MoS_2@PEG, and ET-MoS_2@PEG, respectively, when their concentrations were 150 μg/mL. This suggested that the MoS_2@PEG had good biocompatibility, attributing to the satisfactory biocompatibility of MoS_2 nanosheets and PEG, which was crucial for efficient *in vivo* drug delivery. Simultaneously, both ET and ET-loading MoS_2@PEG showed low cytotoxicity to cells (Figure 2), indicating the anti-inflammatory drug ET was safe for fabricating nanodrugs. No significant *in vitro* cytotoxicity was observed for ET-MoS_2@PEG concentrations of 10-150 μg/mL. Therefore, this noncovalent drug loading approach proved synthetically advantageous because it was typically

achieved via comparatively simple procedures that required fewer chemical reagents, thus reducing the potential for toxicity problems for clinical applications [25,26]. The ET-loading MoS$_2$@PEG concentration of 150 μg/mL, for which no direct cytotoxic effects were observed, was higher than locally administered doses in *in vivo* experiments (100 μg/mL, see below).

In vivo experiments included hematoxylin and eosin (H&E) staining and blood biochemistry analysis; they were also conducted to ensure the safe application of MoS$_2$@PEG and ET-MoS$_2$@PEG. As shown in Figure 3a, the H&E staining showed no obvious tissue damage in the main organs, and significant parameters of blood hematology and biochemistry analysis also indicated no noticeable changes (Figure 3b), in comparison with that of the control groups. Preliminary results provided that MoS$_2$@PEG had low toxicity to our dose tested in mice. The reason for lower toxicity of MoS$_2$@PEG was ascribed to the biocompatible constituents contained in MoS$_2$ and PEG, and their mild synthesis conditions free from toxic organic solvents and chemicals. In addition, the smaller size of as-prepared MoS$_2$@PEG facilitated its body clearances, which may reduce long-term toxicity and could prove beneficial in further bio-applications.

3.3. *In vitro* cellular uptake and anti-inflammatory activity of ET-MoS$_2$@PEG

Cellular uptake is one of the important entry mechanisms for extracellular materials, particularly nanomaterials [27,28]. In this study, the localization of MoS$_2$@PEG in macrophages was investigated by using different fluorescence labels, including F4/80 (red fluorescence, specific targeting to macrophages), DAPI (blue fluorescence, specific targeting to cell nucleus), and green fluorescence protein (GFP) (green fluorescence, specific tagged on MoS$_2$@PEG). Analysis from fluorescence imaging and flow cytometry clearly showed that a larger number (~95.04%) of MoS$_2$@PEG entered into macrophages through cellular uptake approach (Figure 4), which was of great importance to load drugs into SCI sites. This was due to the smaller size of synthesized nanocarriers, which benefited cellular uptake and internalization.

It is known that SCI can induce high expression of TNF-α, a pro-inflammatory

cytokine, which is a key regulator of macrophage polarization [29]. As an effective TNF-α inhibitor, the ET-loading MoS$_2$@PEG is expected to regulate macrophage polarization and further inhibit pro-inflammatory marker expression. It is well-known that LPS is a potent activator of macrophages and is commonly used to activate cells *in vitro* and *in vivo* [22]. Therefore, macrophage activation was induced by treatment with LPS for 6 hours, which created an inflammatory environment *in vitro*. After treating macrophages with LPS, cells were incubated with MoS$_2$@PEG and ET-MoS$_2$@PEG for 2 hours to measure the expressions of pro-/anti-inflammatory markers, respectively. Under cell fluorescence imaging, it showed that MoS$_2$@PEG did not induce the up-regulation of anti-inflammatory (Figure 5a) or pro-inflammatory markers (Figure 5b), compared with PBS group. In contrast, introducing ET-MoS$_2$@PEG obviously led to a lower expression of nitric oxide synthase (iNOS, a classical pro-inflammatory M1 macrophage marker) (Figure 5a), while it promoted a higher expression of arginase 1 (Arg-1, a classical anti-inflammatory M2 macrophage marker) (Figure 5b). This indicated that ET-MoS$_2$@PEG could induce anti-inflammatory M2 macrophage polarization. We further used F4/80 and CD11b to double-label the macrophages, and then investigated the anti-inflammatory activity of ET-MoS$_2$@PEG *in vitro*. The double positive macrophage (F4/80$^+$, CD11b$^+$) polarization of M1/M2 was characterized, and the expressions of M1 and M2 markers were measured by flow cytometry. As shown in Figure 5c-e, low expression of CD11c (M1 marker) was detected in ET and ET-MoS$_2$@PEG groups, compared to PBS and MoS$_2$@PEG groups; however, the ET and ET-MoS$_2$@PEG groups significantly increased the expression of CD206 (M2 marker). Similarly, the analysis from quantitative real-time polymerase chain reaction (RT-PCR) also revealed that ET-MoS$_2$@PEG down-regulated the expression of M1-related TNF-α, CD86, and iNOS markers (Figure 5f), while the expression of M2-related Agr1, CD206 and IL-10 markers were obviously up-regulated (Figure 5g), compared with MoS$_2$@PEG. Collectively, these results demonstrated the anti-inflammatory potential of ET-MoS$_2$@PEG *in vitro,* resulting in M2 macrophage polarization.

3.4. *In vivo* time dependency of ET-MoS$_2$@PEG post-SCI

Adult female mice (C57/BL6) were subjected to a clinically relevant contusion SCI at the thoracic-11 (T11) vertebral level, using a force-controlled impaction device. To determine the permeability of injured spinal cords to MoS$_2$@PEG as a function of time post-injury, we intravenously injected a nanoparticle cocktail comprised of GFP-labeled ET-MoS$_2$@PEG, and then fluorescence imaging was observed at different times post-injury (24, 48, 96 hours and 1 week). As shown in Figure 6, MoS$_2$@PEG extravasates into injured spinal cords after 24, 48, and 96 hours post-injury, respectively. The reason for MoS$_2$@PEG entering into SCI sites was attributed to the breakdown of blood-spinal cord barriers (BSCB) [14], which helped nanomaterials leaking into injured spinal cords. However, at 1 week post-injury, very few nanomaterials were observed in spinal cord tissues (Figure 6d). This indicated that long-circulating drug nanocarriers, such as ET-MoS$_2$@PEG, could achieve efficient drug deliveries even at a 96-hour post-injury time-window. This demonstrated that MoS$_2$@PEG nanoflowers of 200-300 nm in diameter could extravasate into injured spinal cord parenchyma up to 96 hours post-SCI, but not beyond the 1st week post-SCI, which was much longer than the 8 h therapeutic time-window for clinical methylprednisolone (MP) alone. This result showed that using long-circulating nanocarriers such as MoS$_2$ nanocomposites could achieve drug deliveries up to 96 hours post-SCI through passive targeting.

3.5. *In vivo* M1/M2 macrophage polarization and quantitative inflammatory cytokine analysis after ET-MoS$_2$@PEG administration

Macrophages play the important roles in the innate immune responses and, subsequently, tissue repair activities after SCI [30]. Post-injury tissue repair involves regulation of the balance between two major populations of macrophages, including pro-inflammatory M1 and anti-inflammatory M2 macrophages [31]. The M1/M2 ratio is an important factor in SCI repair. M1 macrophages are neurotoxic, while M2 macrophages can promote axonal regeneration after injury [32]. In order to investigate the effects of ET-MoS$_2$@PEG on macrophage polarization, spinal sections from the

1st week post-SCI, mice were characterized using immunofluorescence assay (Figure 7a). Figure 7 presented the changes of local M1/M2 subsets in injured spinal cords *in vivo*. It showed that the ratio of iNOS$^+$/F4/80$^+$ (M1 macrophage marker) was significantly decreased in ET-MoS$_2$@PEG group, while the ratio of Arg1$^+$/F4/80$^+$ cells (M2 macrophage marker) was significantly increased (Figure 7b), when compared with the control groups of ET and MoS$_2$@PEG. *In vivo*, ET group showed a lower expression of anti-inflammatory cytokines, in comparison with *in vitro* anti-inflammatory experiments (Figure 5), which was ascribed to the knowledge that drug molecules were metabolized after blood circulation, and fewer drug molecules could reach injured spinal cords, as shown in the SCI mouse model. These results suggested that ET-MoS$_2$@PEG nanodrugs increased the numbers of M2 macrophages in injured SCI, while reducing the numbers of M1 macrophages; this contributed to modulating inflammatory milieu to a hybrid, anti-inflammatory state.

To assess the expression of inflammation related cytokines, we performed cytokine gene analysis on the spinal cords of the control or ET-MoS$_2$@PEG-treated mice after SCI (Figure 8a). After constructing the model for spinal cord contusions, the mice were treated with PBS, ET, MoS$_2$@PEG, and ET-MoS$_2$@PEG for 24 hours post-SCI, respectively. As shown in Figure 8b, anti-inflammation-associated transcripts, especially interleukins-4 (IL-4) and interleukins-10 (IL-10), were up-regulated on spinal cords of ET-MoS$_2$@PEG-treated mice after SCI, compared with controlled groups. However, pro-inflammation-associated transcripts, including TNF-α, IFN-γ, IL-1α, and IL-6, monocyte chemotactic protein 1 (MCP-1), and macrophage inflammatory protein-1β (MIP-1β), were down-regulated after ET-MoS$_2$@PEG treatment, as shown in SCI model (Figure 8b). Therefore, these results indicated that ET-MoS$_2$@PEG administration could lead to a hybrid, anti-inflammatory condition comprising both promotion of anti-inflammatory cytokine expressions and, simultaneously, inhibition of pro-inflammatory cytokines levels. These results were consistent with anti-inflammatory activity of ET-MoS$_2$@PEG *in vitro*.

3.6. *In vivo* **locomotor recovery and neuroprotective effects**

To further assess locomotor recovery of ET-MoS$_2$@PEG-treated mice after SCI, we measured by a Basso Mouse Scale (BMS) in an open field and analyzed the CatWalk-assisted gait. After constructing a mice model for spinal cord contusions, the mice were treated with PBS, ET, MoS$_2$@PEG, and ET-MoS$_2$@PEG at 48 hours post-SCI, respectively. After traumatic SCI, motor behavior was assessed by BMS in an open field. Complete hindlimb paralysis (BMS score = 0) was observed for all four groups at 1 day post-injury. As shown in Figure 9a, the ET-MoS$_2$@PEG-treated mice exhibited significant improvement in the BMS score (BMS score = 4) at 2-8 weeks post-injury, when compared with control group. Furthermore, the score from the regularity index in ET-MoS$_2$@PEG-treated group was 80 after 8 weeks post-injury (Figure 9b), which was higher than that of ET-treated group.

The CatWalk analysis also showed that the hind maximal contact area after ET-MoS$_2$@PEG treatment was enlarged in 0.12 cm^2, in comparison with 0.08 cm^2 of the ET group (Figure 9c), indicating a significant recovery of hind-limb functions in mice. We further recorded electromyography with a biceps femoris after 8 weeks post-SCI. It showed that the amplitudes of motor-evoked potential (MEP) were significantly higher in ET-MoS$_2$@PEG group (3 mV) than in control groups (Figure 9d).

To further verify the neuroprotective effects of ET-MoS$_2$@PEG, we performed a histological injury study in 8-week post-SCI mice, and the spinal cord tissues were stained using anti-glial fibrillary acidic protein (GFAP) immunostaining. The ET-MoS$_2$@PEG-treated mice had lower injured areas at central lesion sites (Figure 10a), in comparison with the control group, while no notable differences were observed at other regions. Additionally, we stained the neurons with Nissal staining and counted the number of survival motor neurons, as they were responsible for locomotor functions of post-SCI [33]. In comparison with the control groups, a higher number of survival motor neurons were observed on the ET-MoS$_2$@PEG-treated group (Figure 10b). In its entirety, these results demonstrated that the activity of ET-MoS$_2$@PEG was beneficial in SCI treatments because they could provide

neuro-protection and aid in locomotor recovery *in vivo*.

4. Conclusions

In conclusion, the ET-MoS$_2$@PEG nanoflowers have been successfully synthesized as nanodrugs to achieve anti-inflammatory and neuroprotective activities after SCI *in vivo* and *in vitro*. After introducing PEG, MoS$_2$ nanosheets could self-assemble into nanoflowers, exhibited slower drug release, higher payloading capacity, good biocompatibility, and long drug circulation in SCI sites. *In vitro* study suggested that MoS$_2$@PEG nanoflowers were efficient and safe as drug nanocarriers to realize anti-inflammatory macrophage-modulating SCI immunotherapy. Both *in vitro* and *in vivo* studies demonstrated that MoS$_2$@PEG as nanodrugs were capable of up-regulating anti-inflammatory marker expressions via regulating macrophage polarization into anti-inflammatory M2 phenotypes. *In vivo*, the mouse model of SCI showed that ET-MoS$_2$@PEG nanodrugs could extravasate into the injured spinal cord parenchyma up to 96 hours post-SCI, significantly prolonging the time-window for therapy [11,34]. Importantly, anti-inflammatory ET-MoS$_2$@PEG treatments could provide neuro-protection and correspondingly help locomotor recovery, as shown in the mouse model. This study demonstrated the potential of ET-loading MoS$_2$@PEG nanodrugs in SCI immunotherapy.

References

[1] C.S. Ahuja, J.R. Wilson, S. Nori, M.R. Kotter, C. Druschel, A. Curt, M.G. Fehlings, Traumatic spinal cord injury, Nature Reviews Disease Primers 3 (2017) 17018.

[2] L. Schnell, S. Fearn, H. Klassen, M.E. Schwab, V.H. Perry, Acute inflammatory responses to mechanical lesions in the CNS: differences between brain and spinal cord, European Journal of Neuroscience 11 (1999) 3648-3658.

[3] A. Kroner, A.D. Greenhalgh, J.G. Zarruk, R. Passos Dos Santos, M. Gaestel, S. David, TNF and increased intracellular iron alter macrophage polarization to a detrimental M1 phenotype in the injured spinal cord, Neuron 83 (2014) 1098-1116.

[4] K.A. Kigerl, J.C. Gensel, D.P. Ankeny, J.K. Alexander, D.J. Donnelly, P.G. Popovich, Identification of Two Distinct Macrophage Subsets with Divergent Effects Causing either Neurotoxicity or Regeneration in the Injured Mouse Spinal Cord, J Neurosci 29 (2009) 13435-13444.

[5] A. Kroner, A.D. Greenhalgh, J.G. Zarruk, R.P. dos Santos, M. Gaestel, S. David, TNF and Increased Intracellular Iron Alter Macrophage Polarization to a Detrimental M1 Phenotype in the Injured Spinal Cord (vol 83, pg 1098, 2014), Neuron 86 (2015) 1317-1317.

[6] G. Sun, G. Li, D. Li, W. Huang, R. Zhang, H. Zhang, Y. Duan, B. Wang, hucMSC derived exosomes promote functional recovery in spinal cord injury mice via attenuating inflammation, Mater Sci Eng C Mater Biol Appl 89 (2018) 194-204.

[7] R. Shechter, O. Miller, G. Yovel, N. Rosenzweig, A. London, J. Ruckh, K.W. Kim,

E. Klein, V. Kalchenko, P. Bendel, S.A. Lira, S. Jung, M. Schwartz, Recruitment of Beneficial M2 Macrophages to Injured Spinal Cord Is Orchestrated by Remote Brain Choroid Plexus, Immunity 38 (2013) 555-569.

[8] S. Kabu, Y. Gao, B.K. Kwon, V. Labhasetwar, Drug delivery, cell-based therapies, and tissue engineering approaches for spinal cord injury, Journal of Controlled Release 219 (2015) 141-154.

[9] S. Shah, A. Solanki, K.B. Lee, Nanotechnology-Based Approaches for Guiding Neural Regeneration, Acc Chem Res 49 (2016) 17-26.

[10] S. Papa, I. Vismara, A. Mariani, M. Barilani, S. Rimondo, M. De Paola, N. Panini, E. Erba, E. Mauri, F. Rossi, G. Forloni, L. Lazzari, P. Veglianese, Mesenchymal stem cells encapsulated into biomimetic hydrogel scaffold gradually release CCL2 chemokine in situ preserving cytoarchitecture and promoting functional recovery in spinal cord injury, J Control Release 278 (2018) 49-56.

[11] S. Papa, I. Caron, E. Erba, N. Panini, M. De Paola, A. Mariani, C. Colombo, R. Ferrari, D. Pozzer, E.R. Zanier, F. Pischiutta, J. Lucchetti, A. Bassi, G. Valentini, G. Simonutti, F. Rossi, D. Moscatelli, G. Forloni, P. Veglianese, Early modulation of pro-inflammatory microglia by minocycline loaded nanoparticles confers long lasting protection after spinal cord injury, Biomaterials 75 (2016) 13-24.

[12] N. Naderi, D. Karponis, A. Mosahebi, A.M. Seifalian, Nanoparticles in wound healing; from hope to promise, from promise to routine, Front Biosci (Landmark Ed) 23 (2018) 1038-1059.

[13] S. Papa, I. Caron, E. Erba, N. Panini, M. De Paola, A. Mariani, C. Colombo, R.

Ferrari, D. Pozzer, E.R. Zanier, Early modulation of pro-inflammatory microglia by minocycline loaded nanoparticles confers long lasting protection after spinal cord injury, Biomaterials 75 (2016) 13-24.

[14] T. Saxena, K.H. Loomis, S.B. Pai, L. Karumbaiah, E. Gaupp, K. Patil, R. Patkar, R.V. Bellamkonda, Nanocarrier-mediated inhibition of macrophage migration inhibitory factor attenuates secondary injury after spinal cord injury, ACS nano 9 (2015) 1492-1505.

[15] S. Papa, R. Ferrari, M. De Paola, F. Rossi, A. Mariani, I. Caron, E. Sammali, M. Peviani, V. Dell'Oro, C. Colombo, Polymeric nanoparticle system to target activated microglia/macrophages in spinal cord injury, Journal of Controlled Release 174 (2014) 15-26.

[16] Y. Chen, L.Z. Wang, J.L. Shi, Two-dimensional non-carbonaceous materials-enabled efficient photothermal cancer therapy, Nano Today 11 (2016) 292-308.

[17] R. Kurapati, K. Kostarelos, M. Prato, A. Bianco, Biomedical Uses for 2D Materials Beyond Graphene: Current Advances and Challenges Ahead, Advanced Materials 28 (2016) 6052-6074.

[18] X. Li, J.Y. Shan, W.Z. Zhang, S. Su, L.H. Yuwen, L.H. Wang, Recent Advances in Synthesis and Biomedical Applications of Two-Dimensional Transition Metal Dichalcogenide Nanosheets, Small 13 (2017).

[19] R.F. Van Vollenhoven, K. Chatzidionysiou, Rheumatoid arthritis: Triple therapy or etanercept after methotrexate failure in RA?, Nature Reviews Rheumatology 9

(2013) 510-512.

[20] G. Sun, S. Yang, G. Cao, Q. Wang, J. Hao, Q. Wen, Z. Li, K.-F. So, Z. Liu, S. Zhou, γδ T cells provide the early source of IFN-γ to aggravate lesions in spinal cord injury, Journal of Experimental Medicine 215 (2018) 521-535.

[21] N. Liu, Y.L. Guo, X.Y. Yang, H.L. Lin, L.C. Yang, Z.P. Shi, Z.W. Zhong, S.N. Wang, Y. Tang, Q.S. Gao, Microwave-Assisted Reactant-Protecting Strategy toward Efficient MoS2 Electrocatalysts in Hydrogen Evolution Reaction, Acs Applied Materials & Interfaces 7 (2015) 23741-23749.

[22] P.J. Murray, J.E. Allen, S.K. Biswas, E.A. Fisher, D.W. Gilroy, S. Goerdt, S. Gordon, J.A. Hamilton, L.B. Ivashkiv, T. Lawrence, Macrophage activation and polarization: nomenclature and experimental guidelines, Immunity 41 (2014) 14-20.

[23] D.M. Basso, L.C. Fisher, A.J. Anderson, L.B. Jakeman, D.M. McTigue, P.G. Popovich, Basso Mouse Scale for locomotion detects differences in recovery after spinal cord injury in five common mouse strains, J Neurotrauma 23 (2006) 635-659.

[24] G.D. Sun, Y. Chen, Z.G. Zhou, S.X. Yang, C. Zhong, Z.Z. Li, A progressive compression model of thoracic spinal cord injury in mice: function assessment and pathological changes in spinal cord, Neural Regen Res 12 (2017) 1365-1374.

[25] K. Ulbrich, K. Hola, V. Subr, A. Bakandritsos, J. Tucek, R. Zboril, Targeted Drug Delivery with Polymers and Magnetic Nanoparticles: Covalent and Noncovalent Approaches, Release Control, and Clinical Studies, Chem Rev 116 (2016) 5338-5431.

[26] K. Ulbrich, K. Hola, V. Subr, A. Bakandritsos, J. Tucek, R. Zboril, Targeted drug delivery with polymers and magnetic nanoparticles: covalent and noncovalent

approaches, release control, and clinical studies, Chemical reviews 116 (2016) 5338-5431.

[27] S. Wilhelm, A.J. Tavares, Q. Dai, S. Ohta, J. Audet, H.F. Dvorak, W.C. Chan, Analysis of nanoparticle delivery to tumours, Nature reviews materials 1 (2016) 16014.

[28] Y. Li, W. Guo, X. Su, L. Ou-Yang, M. Dang, J. Tao, G. Lu, Z. Teng, Small size mesoporous organosilica nanorods with different aspect ratios: Synthesis and cellular uptake, J Colloid Interface Sci 512 (2018) 134-140.

[29] A. Kroner, A.D. Greenhalgh, J.G. Zarruk, R.P. dos Santos, M. Gaestel, S. David, TNF and increased intracellular iron alter macrophage polarization to a detrimental M1 phenotype in the injured spinal cord, Neuron 83 (2014) 1098-1116.

[30] S. David, A. Kroner, Repertoire of microglial and macrophage responses after spinal cord injury, Nature Reviews Neuroscience 12 (2011) 388-399.

[31] K.A. Kigerl, J.C. Gensel, D.P. Ankeny, J.K. Alexander, D.J. Donnelly, P.G. Popovich, Identification of two distinct macrophage subsets with divergent effects causing either neurotoxicity or regeneration in the injured mouse spinal cord, Journal of Neuroscience the Official Journal of the Society for Neuroscience 29 (2009) 13435.

[32] S.F. Ma, Y.J. Chen, J.X. Zhang, L. Shen, R. Wang, J.S. Zhou, J.G. Hu, H.Z. Lü, Adoptive transfer of M2 macrophages promotes locomotor recovery in adult rats after spinal cord injury, Brain Behavior & Immunity 45 (2015) 157-170.

[33] S. Garbuzova-Davis, C. Kurien, A. Thomson, D. Falco, S. Ahmad, J. Staffetti, G.

Steiner, S. Abraham, G. James, A. Mahendrasah, Endothelial and Astrocytic Support by Human Bone Marrow Stem Cell Grafts into Symptomatic ALS Mice towards Blood-Spinal Cord Barrier Repair, Scientific reports 7 (2017) 884.

[34] F. Papastefanaki, I. Jakovcevski, N. Poulia, N. Djogo, F. Schulz, T. Martinovic, D. Ciric, G. Loers, T. Vossmeyer, H. Weller, M. Schachner, R. Matsas, Intraspinal Delivery of Polyethylene Glycol-coated Gold Nanoparticles Promotes Functional Recovery After Spinal Cord Injury, Molecular Therapy 23 (2015) 993-1002.

Figure legends

Scheme 1. Schematic illustration for (a) the preparation of ET-MoS$_2$@PEG nanoflowers, and (b) their modulated anti-inflammation macrophage in SCI treatment.

Figure 1. Nanostructure characterization and drug delivery of MoS$_2$@PEG nanocomposites. (a) low resolution TEM image, (b) high resolution TEM image, (c) XRD pattern, (c) FT-IR spectra, (d) ET loading on MoS$_2$@PEG and MoS$_2$ nanosheet (n = 3), and (e) *In vitro* release profiles of ET from MoS$_2$ nanosheet and MoS$_2$@PEGs in PBS (pH 7.4) (n = 8).

Figure 2. *In vitro* cell viabilities of MoS$_2$ nanosheets, MoS$_2$@PEGs, ET, and ET-MoS$_2$@PEGs. (a,b) MTT assay of mouse macrophage cell (RAW 264.7) after incubated with different concentrations of nanomaterials (n = 3). (c,d) MTT assay of bone marrow stem cells (BMSC) after incubated with different concentrations of nanomaterials (n = 8).

Figure 3. *In vivo* toxicity evaluation. (a) H&E-stained slice images of major organs, and bars with different characteristics are statistically different at the $P < 0.05$ level. (b) Blood biochemistry data including white blood cells (WBC), red blood cells (RBC), platelets (PLA), Alanine aminotransferase (ALT), aspartate transaminase (AST) and blood urea nitrogen (BUN). (n=8 mice/group).

Figure 4. *In vitro* cellular uptake of MoS$_2$@PEG on macrophages. Fluorescence imaging of (a) DAPI (blue fluorescence), (b) F4/80 (red fluorescence), (c) GFP-labeled PEG@MoS$_2$ (green fluorescence), (d) the merging fluorescence. Fluorescence quantitative analysis by flow cytometry (e). Scale is 100 μm.

Figure 5. *In vitro* anti-inflammatory activity of ET-MoS$_2$@PEG on LPS-mediated activated macrophages. (a) Fluorescence imaging showed MoS$_2$@PEG administration induced low expression of M1-related pro-inflammatory marker. Scale is 50 μm. (b) Fluorescence imaging showed MoS$_2$@PEG administration induced high expression of M2-related anti-inflammatory marker. (c-e) Flow cytometry analysis for the expression of CD11c (mark of M1) and CD206 (mark of M2) on macrophage (F4/80$^+$, CD11b$^+$) (n = 8). (f, g) RT-PCR quantitative analysis of M1 and M2 macrophage

marker expression on activated macrophages (n = 8). *, $P < 0.05$; **, $P < 0.01$; ***, $P < 0.001$.

Figure 6. *In vivo* ET-MoS$_2$@PEG extravasation is dependent on time post-SCI. Fluorescence imaging of injured spinal cord at 24 hours (a), 48 hours (b), 96 hours (c) and 1 week (d) post-injury.   (n=6 mice/group).

Figure 7. *In vivo* M1/M2 macrophage polarization after ET-MoS$_2$@PEG administration. (a,b) Spinal sections from the mice after 1 week post-SCI were immunostained with anti-F4/80 (red, a generic marker for macrophages), anti-iNOS (green, a maker for M1 macrophages) and anti-Arg1 (green, a maker for M2 macrophages). Scale bar 100 μm, ***$P < 0.001$. Means ± SEM. (n = 6 mice/group).

Figure 8. *In vivo* quantitative inflammatory cytokine analysis. (a) Pro-inflammatory cytokines in spinal samples were analyzed using the luminex analysis system (Bio-Rad, Hercules, CA) at 24 hours after SCI. Different colors indicated the protein levels from low (blue) to high (red) representing the fold change. (b) ET-MoS$_2$@PEG treatment significantly increased anti-inflammatory markers IL-4 and IL-10 levels, while decreased pro-inflammatory markers such as TNF-α, IFN-γ, IL-1α, IL-6, MCP-1, and MIP-1β. *, $P < 0.05$; **, $P < 0.01$; ***, $P < 0.001$. (n = 6 mice/group).

Figure 9. *In vivo* locomotor recovery after ET-MoS$_2$@PEG administration. (a) BMS scores at different time-points after spinal cord contusion (n=8 mice/group). (b) Regularity Index at different time-points. (c) Hind Max Contact Areas were analyzed using the CatWalk XT automated quantitative gait analysis system (n=8 mice/group). (d) Examples and the statistic histogram of motor-evoked potential (MEP) recordings from mice 8 weeks post-surgery (n=8 mice/group), *, $P < 0.05$; ***, $P < 0.01$.

Figure 10. ET-MoS$_2$@PEG reduced damaged area and protected neurons after SCI. (a) Representative injury sites labeled with anti-GFAP antibodies and the statistic histogram of lesion volumes in different groups (n=8 mice per group; Scale bar: 500 μm). (b) Survival of motor neurons immunostained with Nissl staining in the spinal cord ventral horn (VH) at the 8 week after SCI. (n=8 mice/group; Scale bar: 50 μm). *, $P < 0.05$; ***, $P < 0.001$.
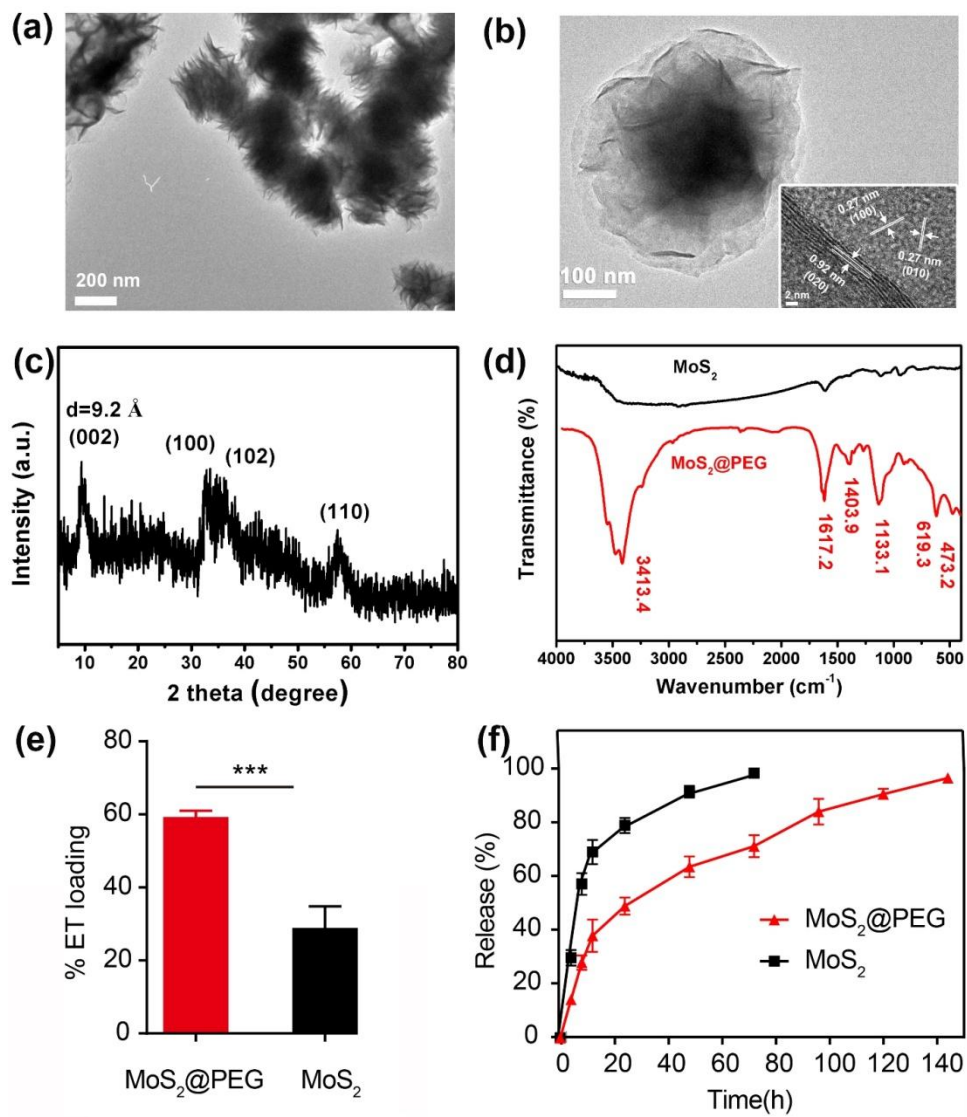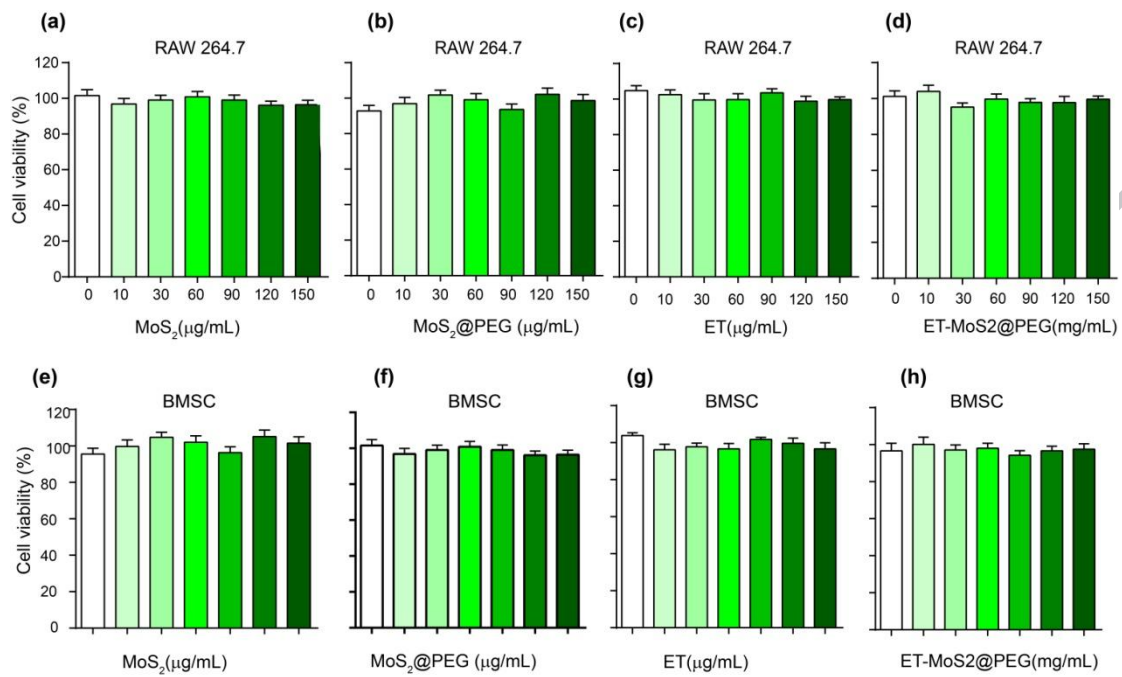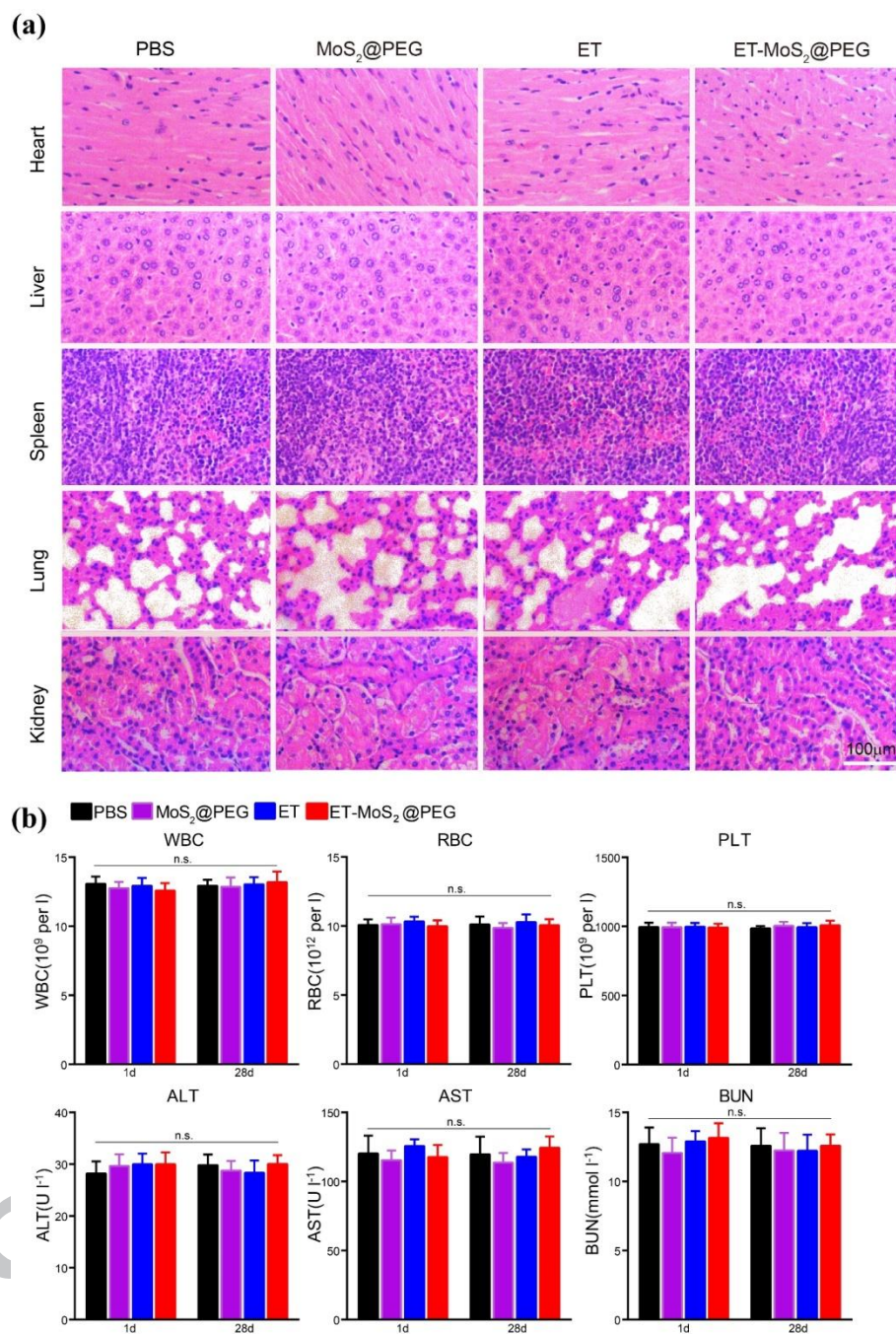
Figures
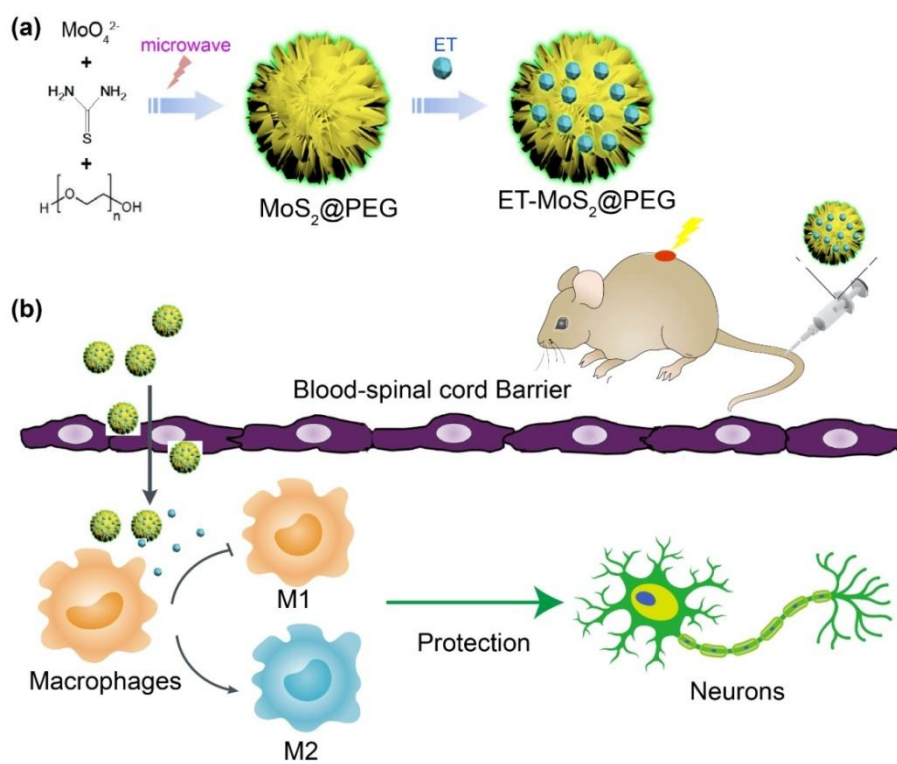
Scheme 1

Figure 1

Figure 2

Figure 3
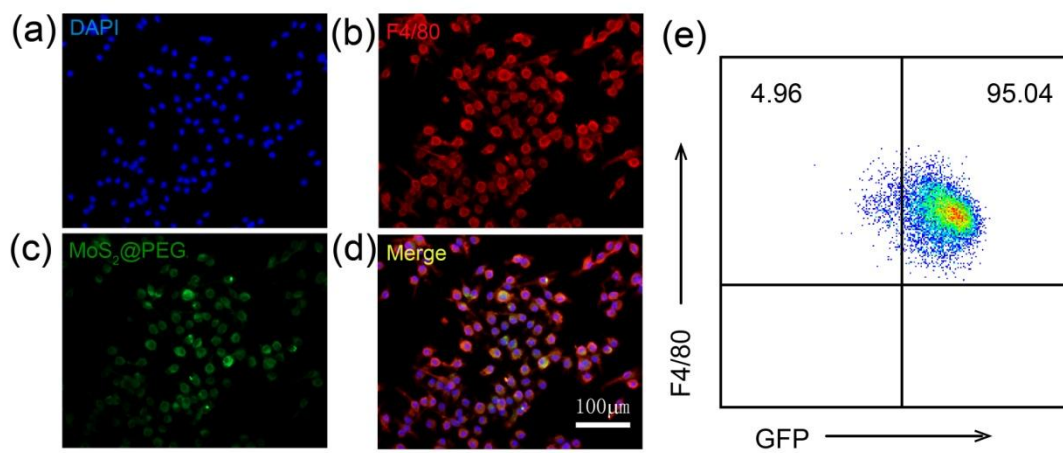
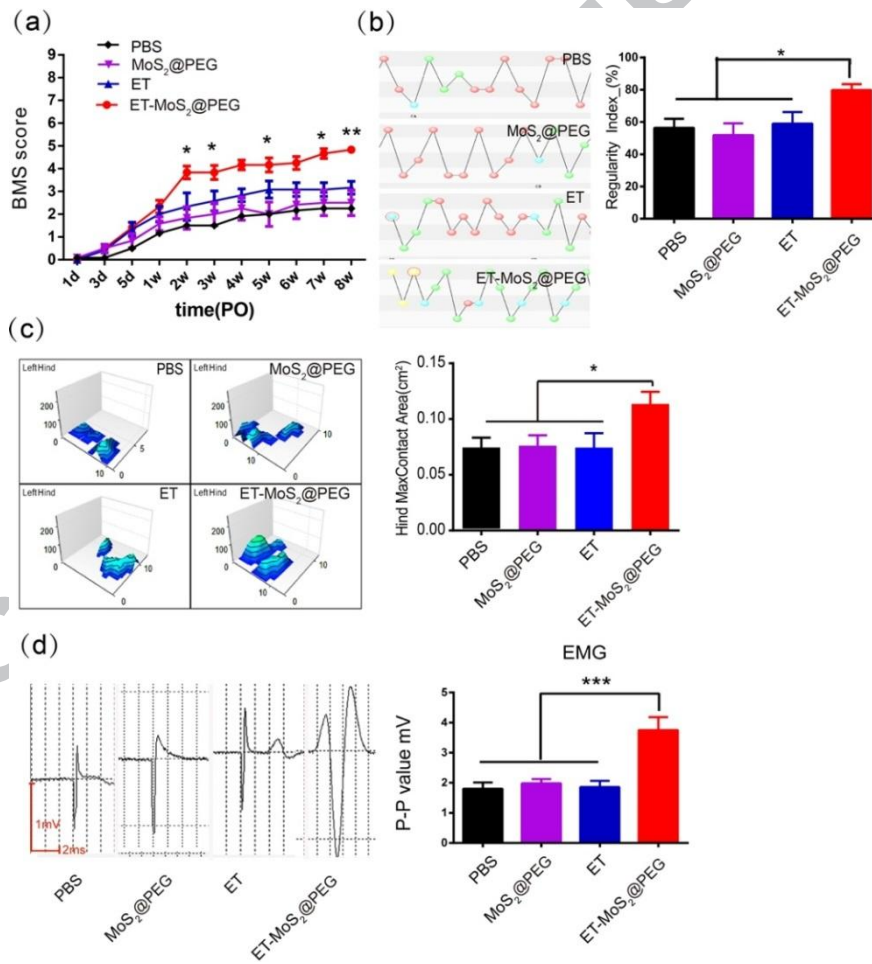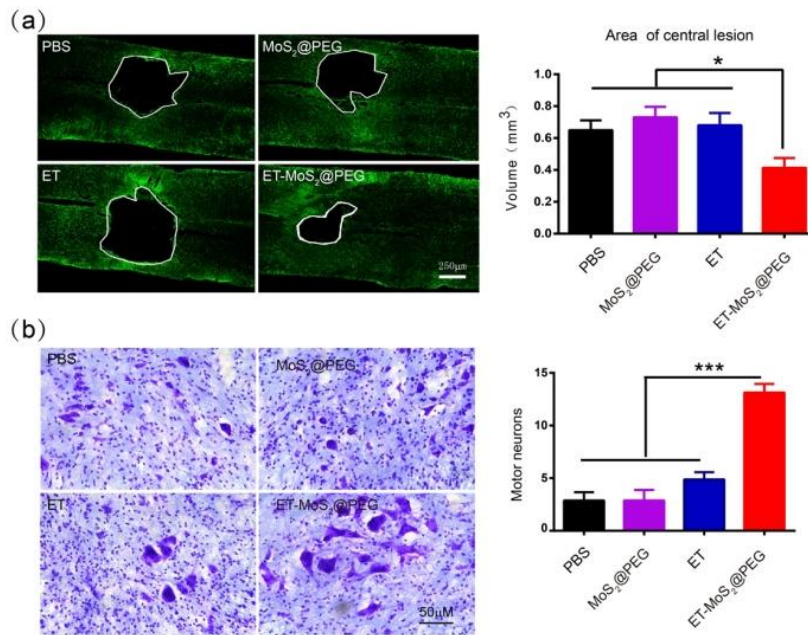**Figure 4**
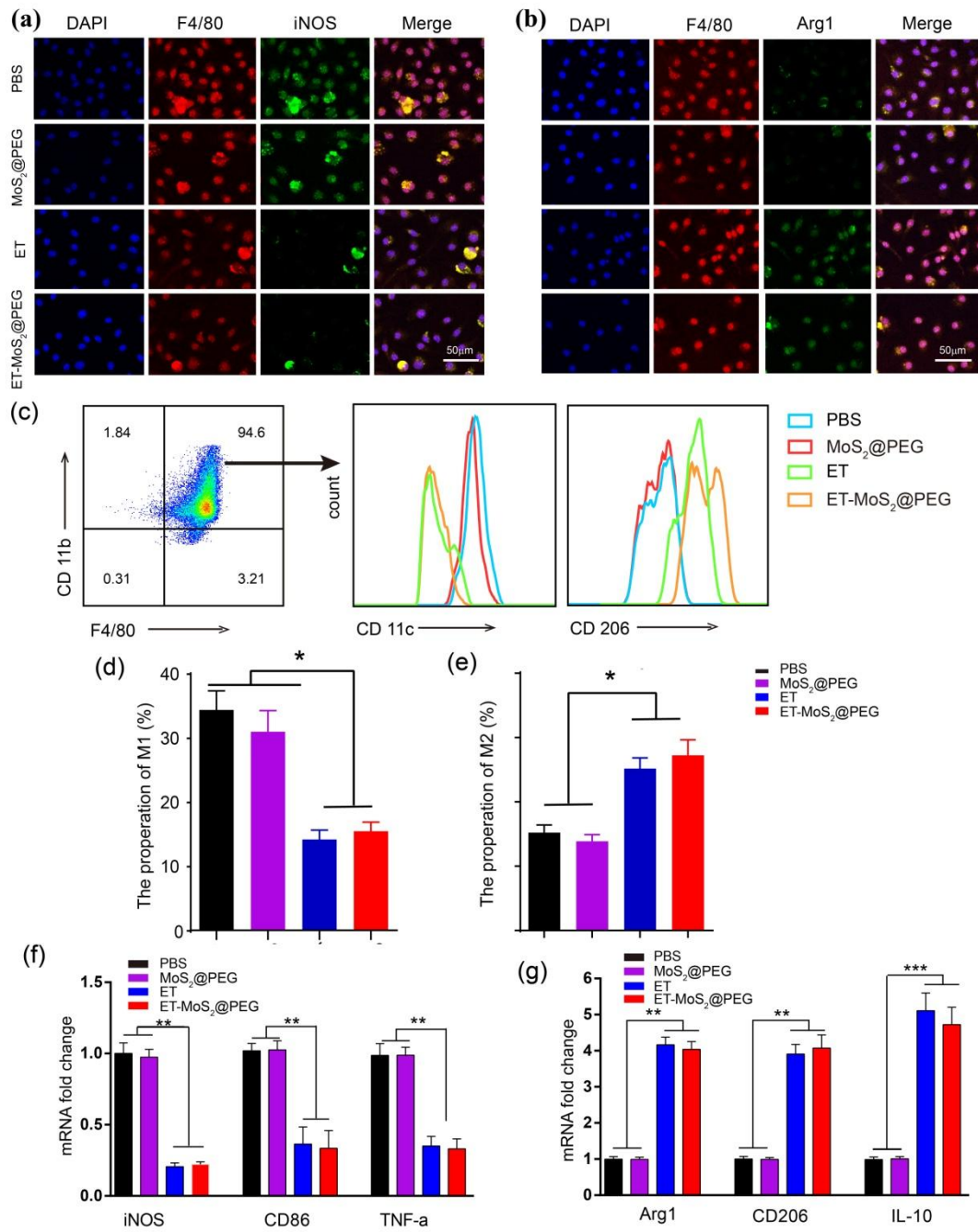
Figure 5
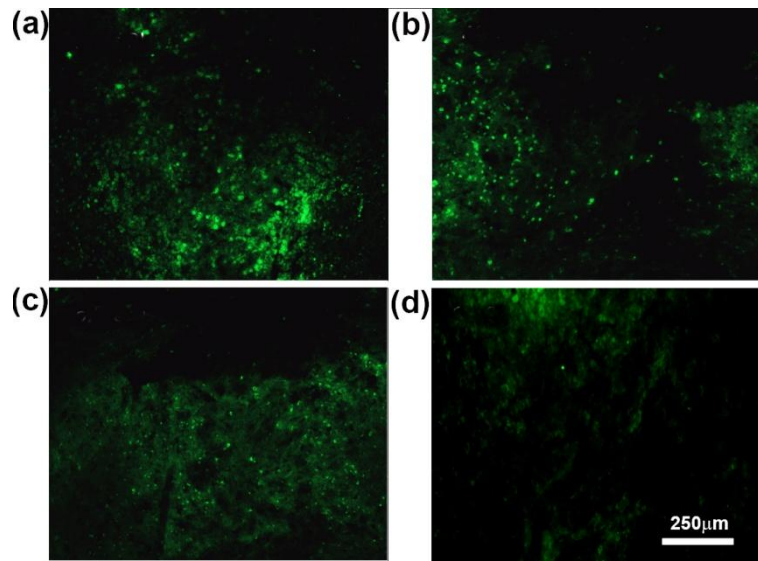
Figure 6
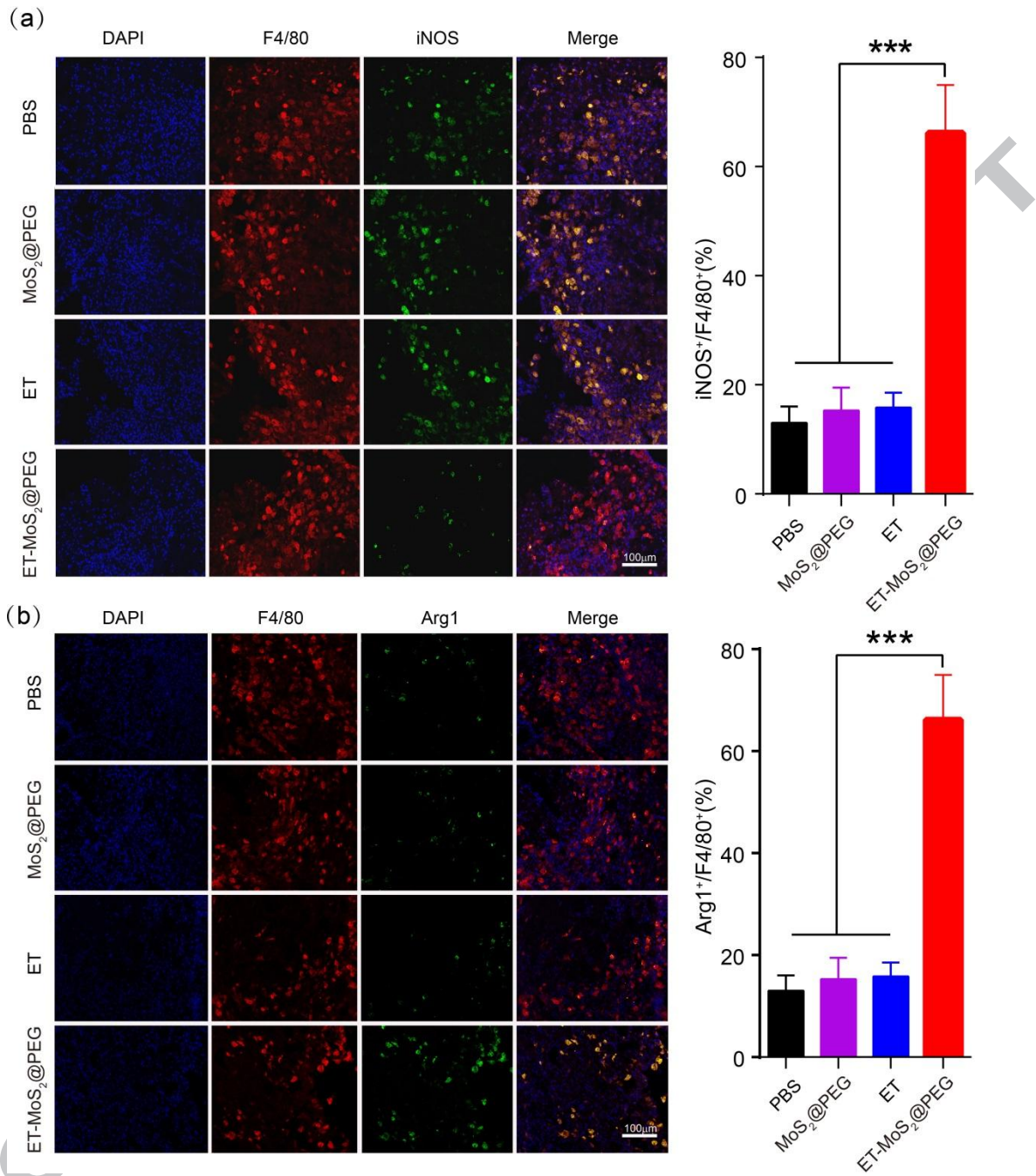
Figure 7
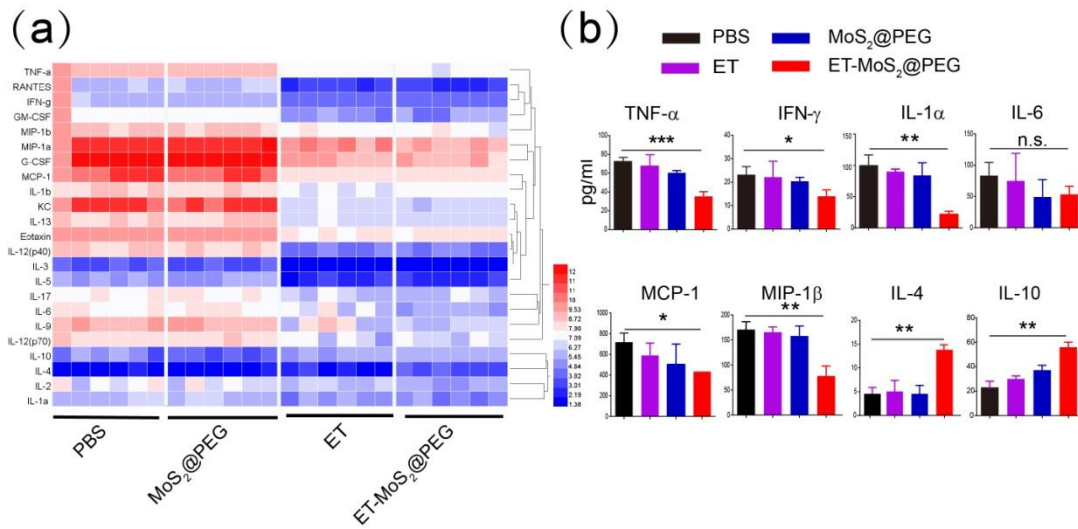
Figure 8

Figure 9

Figure 10

Graphical abstract